IOP Publishing Measurement Science and Technology

Meas. Sci. Technol. **19** (2008) 065704 (7pp) doi:10.1088/0957-0233/19/6/065704

A quartz crystal microbalance technique to study wax crystallization in the presence of gas

M Cassiède[1], J Pauly[1], M Milhet[1], M Rivaletto[2], I M Marrucho[3], J A P Coutinho[3] and J-L Daridon[1]

[1] Laboratoire des Fluides Complexes, UMR 5150, BP 1155, 64013 Pau Cedex, France
[2] Laboratoire de Génie Electrique, Hélioparc Pau-Pyrénées, 64053 Pau Cedex 9, France
[3] CICECO, Universidade de Aveiro, 3810-193 Aveiro, Portugal

E-mail: cassiede.marc@etud.univ-pau.fr

Received 4 February 2008, in final form 8 April 2008
Published 8 May 2008
Online at stacks.iop.org/MST/19/065704

Abstract
A quartz crystal microbalance (QCM) was designed to measure the melting temperature in the presence of gas under high pressure. The capacity of the experimental technique to determine the liquid–solid as well as the solid–solid transitions was first tested by measuring the phase transition temperatures of several pure *n*-alkanes from *n*-C_{19} to *n*-C_{30} under atmospheric pressure and by comparing the results with literature data. Then, the wax disappearance conditions were determined for linear alkanes from *n*-C_{20} to *n*-C_{22} in the presence of carbon dioxide under pressure. The resulting solid–liquid–vapour three-phase equilibrium curves correctly match those obtained in earlier studies.

Keywords: quartz crystal microbalance, phase transitions, solid–liquid–vapour equilibria, *n*-alkanes, carbon dioxide

(Some figures in this article are in colour only in the electronic version)

1. Introduction

Accurate knowledge of the phase behaviour of pure *n*-alkanes or waxy mixtures represents a major scientific concern in petroleum engineering. The alkanes are saturated hydrocarbon compounds that count among the main components of the oil fluids and are responsible for the paraffinic deposits due to their high melting points. It is thus important to know the conditions of phase change (pressure and temperature) of these systems in order to prevent the formation of solid deposits intervening during their production and their transport [1].

In transparent systems, the appearance or disappearance of microcrystals in a homogeneous phase characterizing the beginning or the end of the crystallization can be easily detected by microscopic or even direct visual observation up to pressures of 100 MPa [2–4]. However, in opaque systems, visual methods do not work and the phase transitions must be determined indirectly. For this purpose, discontinuities or breaks in the representative curves of some physical properties of the material are identified as the temperature, pressure or composition of the system are changed. Numerous methods have already been developed to study the variation of properties such as the viscosity [5, 6], the speed of sound [7, 8], the transmitted light power [9] through the studied sample or the liberated heat flux [10]. Unfortunately, most of these techniques do not give accurate values when liquid–solid phase transitions do not lead to sharp effects [11]. Furthermore, most of the usual techniques working under pressure require a large amount of material and cannot be used when sample amounts are limited. Therefore, new techniques which allow waxy solid–liquid phase transition measurements with a small amount of wax in the presence of high-pressure gases need to be designed. With this aim in mind, we decided to test the capacities of the quartz crystal microbalance technique to measure the wax appearance conditions under pressure. A high-pressure quartz microbalance was already implemented to study low gas solubilities in polymers [12, 13]. In this work, we have extended the investigation

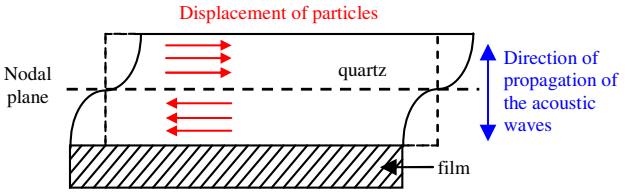

Figure 1. Shear waves in a quartz crystal.

range of this previous apparatus. In order to check the ability of the apparatus to detect solid–solid as well as solid–liquid transitions, measurements were first carried out at atmospheric pressure on several pure *n*-alkanes ranging from *n*-C_{19} to *n*-C_{30} and the temperature values were compared with those obtained by several authors in the literature. Then, the solid–liquid–vapour three-phase equilibrium curve for the binary systems {CO_2 + *n*-C_{20}}, {CO_2 + *n*-C_{21}} and {CO_2 + *n*-C_{22}} has been determined.

2. Experimental details

2.1. Experimental technique

The principle of the quartz crystal microbalance (QCM) is based on the piezoelectric effect. The system is mainly composed of a thin quartz strip sandwiched between two metallic electrodes. By applying a periodic electric current to the quartz crystal, it is submitted to periodic mechanical constraints and sound waves appear. Shear waves can be generated from the electrodes and cross the crystal involving a shear displacement of particles [14]. On both sides of the nodal plane, the planes parallel to the surface move in opposite directions (figure 1).

The system then enters into resonance and starts to oscillate. The resonant frequency of the quartz crystal f_n for each odd harmonic of order n is given by [15]

$$f_n = \frac{n v_q}{2 d_q}. \tag{1}$$

Since v_q represents the velocity of propagation of the acoustic waves in quartz, the resonant frequency is mainly given by the thickness of the crystal d_q. Moreover, the crystal starts resonating when the wavelength λ_n is a multiple of twice the thickness of quartz:

$$n\lambda_n = 2d_q. \tag{2}$$

The frequency at which the amplitude of vibration of the acoustic waves is maximum is called the fundamental resonant frequency of quartz and is denoted f_0. In this case, the crystal is not subjected to any interaction with the surrounding medium.

These oscillations are extremely sensitive to any change intervening on the surface of the crystal and particularly to a small gain or loss of mass on the electrodes [16]. The quartz crystal is also sensitive to other parameters such as the temperature, the contact with a viscous fluid and the pressure [17]. The contributions of each factor to the frequency shift are additive:

$$\Delta f = \Delta f_m + \Delta f_T + \Delta f_\eta + \Delta f_P. \tag{3}$$

Thus, modifications of the frequency of the acoustic waves being propagated in the crystal indicate changes of the properties at the surface of the resonator. In particular, when a layer is uniformly deposited on an electrode, the thickness of the resonator increases and consequently f_n decreases. This frequency decrease depends on the thickness of the additional layer [18] but also on the shear modulus of the material [19, 20]. Consequently, when a liquid–solid phase transition appears inside the attached layer, the viscoelastic properties of the sample hugely change and the oscillation frequency of the resonator is modified. Therefore, the monitoring of the resonant frequency during a temperature scan can be used to determine liquid–solid phase transitions by the appearance of a sharp break in the curve [21, 22].

2.2. Experimental device

The experimental apparatus is built around an autoclave cell made up of a stainless steel block designed to resist pressures as high as 100 MPa (figure 2).

The cell can contain two quartz crystals. Each of them is connected to an integrated circuit Motorola MC12061 [23] to form a crystal-controlled oscillator (figure 3).

Its output generates an electrical TTL signal at the eigenfrequency of the external crystal. This output is connected to an Agilent 53131A frequency counter. The circuit has an automatic gain control (AGC) and its frequency stability versus the temperature variation (crystal held at a constant temperature) is about -0.08 ppm $^\circ C^{-1}$ around 8 MHz. The quartz crystals used in this work vibrate in the thickness shear mode as described above, at different fundamental frequencies f_0 ranging between 5 MHz and 9 MHz.

The temperature of the whole cell is regulated by an oven within the range 263.15–373.15 K. The crystal oscillator operates in the temperature range 273.15–343.15 K. The temperature is measured by means of a platinum resistance temperature detector inserted inside a hole made in the cell and situated close to the crystals. The uncertainty of temperature values is estimated at 0.2 K.

The gas is transmitted to the cell through a hand pump and the pressure is controlled with a manometer, with a precision of 0.02%.

2.3. Experimental procedure

As the studied samples are in solid state at ambient temperature and atmospheric pressure, they are first dissolved and then deposited uniformly on the surface of an electrode covering the crystal. Due to important subcooling effects during crystallization, the phase change between the high temperature solid phase and the liquid phase is determined by measuring the disappearance conditions of the last crystals instead of the crystallization onset. Consequently, the samples are slowly heated with a temperature gradient of 0.15 K min^{-1} until the melting of the material.

The gas is injected into the cell at the highest possible pressure, near the upper critical end point (UCEP) of the triphasic curve, and at sufficiently low temperatures to remain in the solid–vapour equilibrium area. Once the gas is

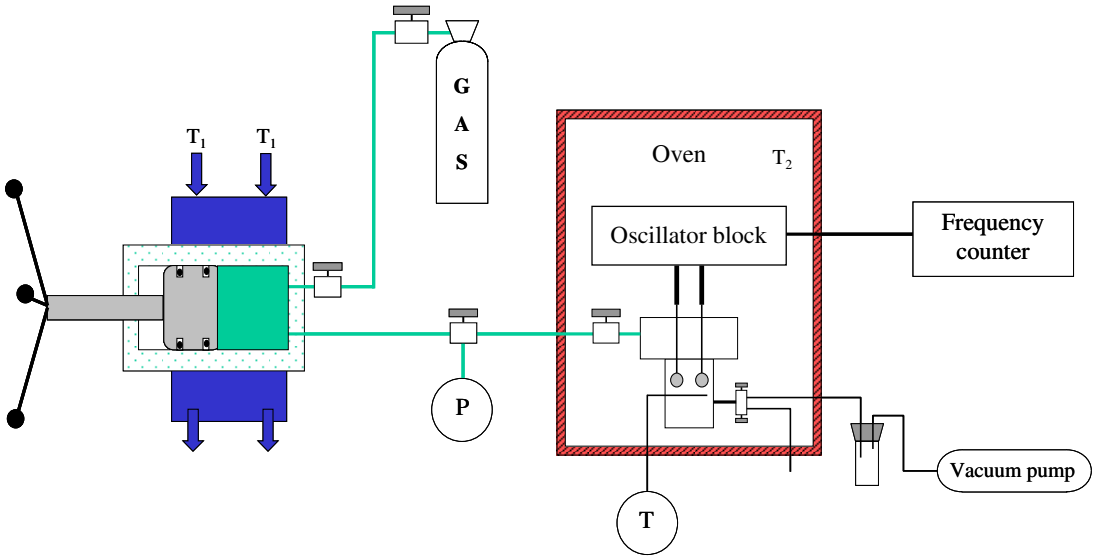

Figure 2. Overall diagram of the experimental device.

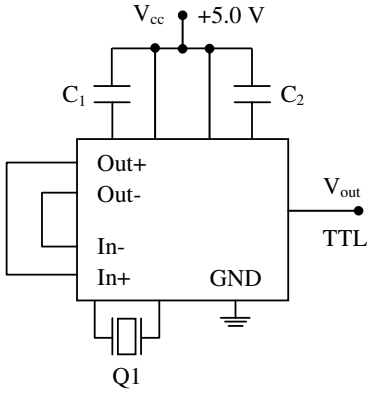

Figure 3. Schematic circuit of the crystal oscillator.

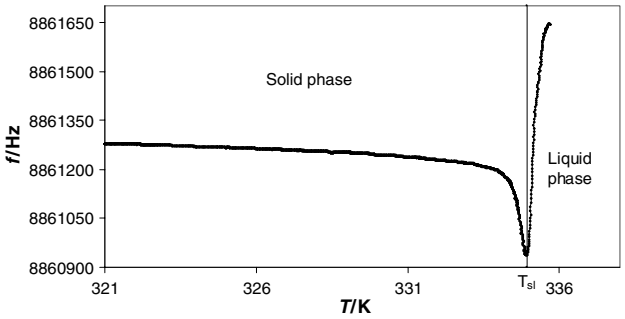

Figure 4. Frequency variation of quartz coated with n-C_{29} as a function of temperature.

solubilized in the solid component and the system is stabilized, the mixture is slowly heated in an isobaric process. When the sample becomes liquid, the pressure is decreased to recrystallize the material. Heating is carried out again until melting.

2.4. Chemicals

The pure linear alkanes used in this work were purchased from ALDRICH and FLUKA, with purities better than 99 wt% for most of the components. Only n-C_{22}, n-C_{23} and n-C_{27} have a purity lower than 99 wt%. The carbon dioxide was obtained from MESSER, with a purity rating of 99.995 vol%. All the compounds were used without any further purification.

3. Results and discussion

3.1. Study of pure n-alkanes from n-C_{19} to n-C_{30}

When the added layer is solid (low temperature phase), its shear modulus is high and thus the material vibrates synchronously with the quartz crystal. In figure 4 is shown the oscillation frequency curve versus temperature of a crystal coated with a sample of n-C_{29}.

Equation (3) and the characteristics of the integrated circuit can explain the fact that the resonant frequency decreases with temperature. On the condition that the deposited mass is small compared to the mass of the quartz, the deviation from the fundamental frequency Δf can be expressed according to Sauerbrey's equation [18] :

$$\Delta f = \frac{-2 f_0^2 \Delta m}{A_0 Z_{cq}} = -k\ \Delta m, \qquad (4)$$

where Z_{cq} is the characteristic quartz impedance and $\frac{\Delta m}{A_0}$ represents the added mass per unit area.

Consequently, changes in density and thickness of the layer can cause frequency variations. Thus, the drop observed of a few tenths of a degree before the melting temperature can be attributed to molecular rearrangements [24].

When the material starts melting, a significant frequency increase is observed. Indeed, when the sample is liquid, the shift from the fundamental frequency follows the Kanazawa

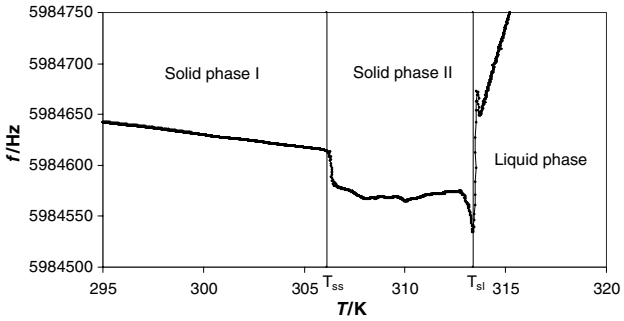

Figure 5. Frequency variation of quartz coated with n-C_{21} as a function of temperature.

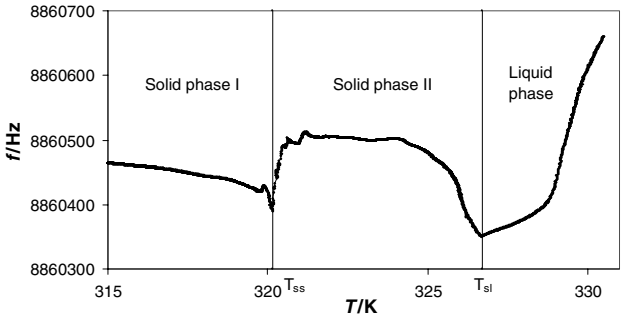

Figure 6. Frequency variation of quartz coated with n-C_{25} as a function of temperature.

relation [20]:

$$\Delta f = -\frac{f_0^{3/2}}{Z_{cq}\sqrt{\pi}}\sqrt{\rho_l \eta_l}, \tag{5}$$

where η_l and ρ_l are the viscosity and density of the liquid, respectively. Besides, it is proved that most petroleum fluids exhibit Newtonian behaviour as soon as their temperature is above the crystallization point. Newtonian fluids follow an Arrhenius temperature dependence. Their dynamic viscosity η is given by the Andrade law:

$$\eta = \eta_0 \exp\left(\frac{E_a}{RT}\right). \tag{6}$$

The increase in the resonant frequency of quartz beyond the melting temperature thus reveals the Arrhenius behaviour of n-alkanes. So, this criterion of determination of the liquid–solid transition has been applied for each linear alkane from n-C_{19} to n-C_{30}.

The frequency curves of most of the compounds present discontinuities below the melting temperature which reveal some structural changes or some destabilizations.

After this abrupt change, the system tends to come back to an equilibrium, which results in a stabilization of the oscillation frequency. The temperature at which this phenomenon appears corresponds to the solid–solid transition temperature between the ordered crystal phase and the disordered rotator phase. Many crystallographic studies [24] conducted by using calorimetry or x-ray diffraction have revealed three categories of polymorphous phases in solid n-paraffins: the ordered phases of low temperatures, the ordered phases of high temperatures and the disordered phases of high temperatures, named rotator phases. The order–disorder solid–solid transition induces significant changes in the orientation of molecules, leading to an important enthalpy variation and a modification of the layer density. Moreover, the existence of some defects in both solid structure and film adhesion can cause strong effects during solid–solid phase transitions. Interplays of all these factors lead to abrupt changes in the resonant frequency. However, according to the amplitude of each effect, either a decrease (figure 5) or an increase (figure 6) in frequency can be observed. On the other hand, the transitions occurring in the ordered and disordered phases are accompanied by low thermal effects and few modifications of the molecular structure, so they are

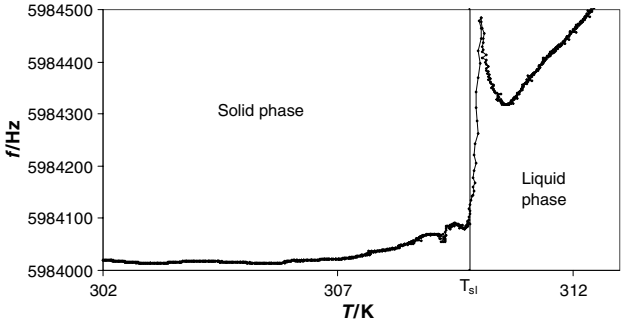

Figure 7. Frequency variation of quartz coated with n-C_{20} as a function of temperature.

usually difficult to detect by calorimetry. Nevertheless, it can be observed that the QCM can pick up this kind of transition in the rotator phase in a narrow temperature range before melting by the presence of a slope change in the frequency curve (figures 4 and 5). Thus, the method enables one to measure both liquid–solid and solid–solid transitions.

For n-C_{20}, a short discontinuity was observed just before the melting point that was not considered in this work (figure 7). Some authors indicate the existence of a solid–solid transition which could correspond to the small peak detected [25, 26].

For some compounds, such as n-C_{20} and n-C_{21}, the solid–liquid transition leads to a huge increase in frequency, followed by a small drop in frequency before the system comes back to the regular behaviour. This repeatable phenomenon may be related to strong thermal effects induced by the melting of the sample. The minimum corresponds to the return to thermal equilibrium of the system.

The measurements of both solid–liquid (S–L) and solid–solid (S–S) transition temperatures performed at atmospheric pressure on 12 paraffins ranging from n-C_{19} to n-C_{30} are reported in table 1 and plotted in figure 8 along with values given by Broadhurst [27].

Our results correctly match the data reported by Broadhurst [27]. The validity of this experimental method was checked by comparison with all literature data [27–31] available at atmospheric pressure as summarized in tables 2 and 3.

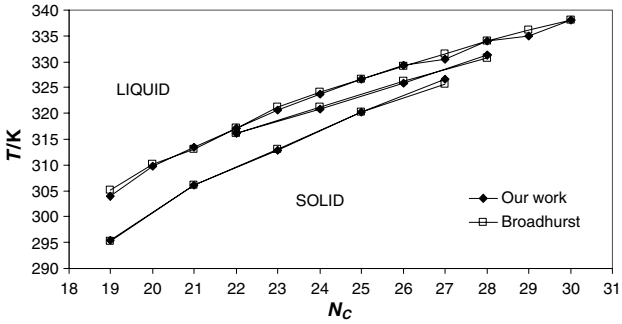

Figure 8. Phase transition temperatures of pure *n*-alkanes with carbon number 19 to 30. The lowest curve connects the S–S structure transition temperatures for *n*-alkanes with odd carbon number, the curve above connects the S–S transition temperatures for *n*-alkanes with even carbon number and finally, the highest curve connects the melting temperatures for each component.

Table 1. Solid–solid and solid–liquid phase transition temperatures T_{ss} and T_{sl} for *n*-alkanes with carbon number 19–30.

N_C	Purity (wt%)	T_{ss} (K)	T_{sl} (K)
19	99.0	295.5	304.0
20	99.0		309.8
21	99.5	306.1	313.4
22	98.0	316.2	317.2
23	98.0	312.8	320.7
24	99.0	320.9	323.7
25	99.0	320.2	326.7
26	99.0	325.9	329.4
27	98.0	326.7	330.5
28	99.0	331.3	333.9
29	99.5		335.0
30	99.0		338.1

Table 2. Deviations between experimental solid–solid phase transition temperatures T_{ss} of pure *n*-alkanes with carbon number 19–30 and literature data T_{ref}.

N_C	$T_{ss} - T_{ref}$ (K)		
19	0.35^{27}	0.35^{30}	-0.45^{31}
20			
21	-0.05^{27}	0.40^{28}	0.45^{31}
22	0.05^{27}	0.75^{30}	0.05^{31}
23	-0.35^{27}	-0.35^{30}	-0.85^{31}
24	-0.25^{27}	0.65^{30}	-0.35^{31}
25	0.05^{27}	0.95^{30}	0.05^{31}
26	-0.25^{27}	0.55^{30}	-0.55^{31}
27	0.95^{27}	-0.15^{30}	0.55^{31}
28	0.55^{27}	0.35^{29}	0.15^{31}

The average deviation is 0.13 K for both solid–solid and solid–liquid transition temperatures whereas the absolute deviation observed is about 0.4%. It is worth mentioning that literature data present, in some cases, uncertainties larger than 1 K. In order to better analyse such differences between our results and literature data, we compared the average deviation of our measurements to the average deviation of literature data for each component. The value calculated in this way is inferior to 0.1 K for both transitions. These results demonstrate the capacity of this technique to determine liquid–solid and solid–solid transitions in waxy systems. Despite the fact that the temperature probe is not stuck to the quartz oscillator but only located close to it, the temperature measurements are in agreement with literature data. Based on this comparison we can consider an accuracy of about 0.2 K for the transition temperatures measured in this work.

Table 3. Deviations between experimental solid–liquid phase transition temperatures T_{sl} of pure *n*-alkanes with carbon number 19–30 and literature data T_{ref}.

N_C	$T_{sl} - T_{ref}$ (K)			
19	-1.15^{27}	-1.20^{28}	0.05^{30}	-1.15^{31}
20	-0.35^{27}		0.75^{30}	
21	0.25^{27}	-0.30^{28}		0.05^{31}
22	0.05^{27}		1.45^{30}	0.05^{31}
23	-0.45^{27}		0.75^{30}	0.05^{31}
24	-0.45^{27}		0.65^{30}	-0.05^{31}
25	0.00^{27}		0.85^{30}	0.05^{31}
26	0.25^{27}		0.45^{30}	-0.05^{31}
27	-1.05^{27}	-0.45^{29}	-0.65^{30}	-1.45^{31}
28	-0.05^{27}	-0.05^{29}	0.35^{30}	-0.45^{31}
29	-1.15^{27}	1.35^{29}		-1.55^{31}
30	-0.05^{27}	0.05^{29}	0.25^{30}	-0.45^{31}

3.2. Study of {CO_2 + n-alkane} binary systems

Taking into account the good results obtained at atmospheric pressure, measurements were extended to high pressure by adding some gas. According to Gibb's phase rule, the coexistence of three phases corresponds to a monovariant state for a binary system. Thus, the measurement of the melting temperature of a paraffin in the presence of gas corresponds to the determination of the solid–liquid–vapour three-phase temperature at a fixed pressure. Consequently, the examination of the frequency curve of a quartz crystal coated with a pure wax in the presence of gas enables the determination of the solid–liquid–vapour *P–T* line. These curves are usually obtained visually or by noting the intersections of the solid–liquid and liquid–vapour two-phase boundary curves. Carbon dioxide was chosen for this investigation and the solid–liquid–vapour equilibrium lines for the three binary systems {CO_2 + *n*-C_{20}}, {CO_2 + *n*-C_{21}} and {CO_2 + *n*-C_{22}} were studied. Measurements performed on these systems are reported in table 4 and plotted in figure 9 where they are compared to earlier studies for both {CO_2 + *n*-C_{21}} and {CO_2 + *n*-C_{22}} systems [32, 33].

It can be observed that the measurements performed on {CO_2 + *n*-C_{21}} perfectly match the literature data whereas {CO_2 + *n*-C_{22}} data present some deviations (of about 1 K) from the data of Fall *et al* (1984) as the pressure increases.

These results show that the QCM technique enables measurements of solid–liquid–vapour three-phase equilibrium lines of binary systems as well as solid–liquid transitions of pure components. However, the measurements become increasingly difficult as conditions approach the upper critical end point (UCEP). In this domain, the solubility of waxes in fluid phase is significant. The wax initially coating the quartz crystal tends to solubilize in the gas phase. Due to the small amount of wax laid on the crystal, this phenomenon

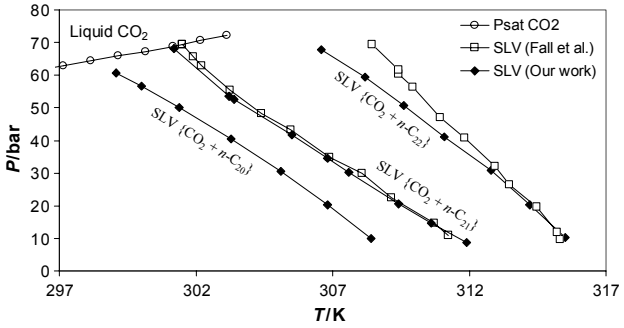

Figure 9. SLV curves for {CO_2 + *n*-alkane} binary systems.

Table 4. Solid–liquid–vapour equilibrium point of {CO_2 + *n*-alkane} binary systems at different pressures.

{CO_2 + *n*-C_{20}}		{CO_2 + *n*-C_{21}}		{CO_2 + *n*-C_{22}}	
P (bar)	T_{slv} (K)	*P* (bar)	T_{slv} (K)	*P* (bar)	T_{slv} (K)
10.1	308.4	8.6	311.9	10.3	315.5
20.1	306.8	14.7	310.6	20.2	314.2
30.4	305.1	20.7	309.4	30.7	312.8
40.4	303.3	30.2	307.6	41.2	311.1
50.1	301.4	34.6	306.8	50.7	309.6
56.7	300.0	41.6	305.5	59.3	308.2
60.7	299.1	52.5	303.4	67.9	306.6
		53.5	303.2		
		68.2	301.2		

can lead to the full disappearance of wax from the QCM before melting, making the technique non-operative. In order to avoid such difficulties while doing measurements close to UCEP, the volume of gas must be reduced and saturated with paraffins before introduction into the cell and finally wax must be added in excess in the bottom of the cell. By adopting these procedures, the QCM technique is revealed to be promising with regard to the quartz response in a gaseous medium and it offers interesting prospects to study phase equilibria of systems with low solubilities.

4. Conclusion

A quartz crystal microbalance device under pressure was developed and then validated by determining the phase transition temperatures of 12 pure *n*-alkanes from *n*-C_{19} to *n*-C_{30}. Our results proved to be in very good agreement with the data of the specialized literature. The first use of the experimental device under pressure consisted in establishing the three-phase equilibrium curve solid–liquid–vapour of binary systems composed of carbon dioxide and a linear alkane from *n*-C_{20} to *n*-C_{22}. It is shown that the results correctly match those obtained in earlier studies.

References

[1] Misra S, Baruah S and Singh K 1995 Paraffin problems in crude oil production and transportation: a review *SPE Prod. Facil.* **10** 50–4

[2] Milhet M, Pauly J, Coutinho J A P, Dirand M and Daridon J L 2005 Liquid–solid equilibria under high pressure of tetradecane + pentadecane and tetradecane + hexadecane binary systems *Fluid Phase Equilibria* **235** 173–81

[3] Milhet M, Pauly J, Coutinho J A P and Daridon J L 2007 Solid–liquid equilibria under high pressure of eight pure *n*-alkylcyclohexanes *J. Chem. Eng. Data* **52** 1250–4

[4] Milhet M, Pauly J, Coutinho J A P and Daridon J L 2008 Solid–liquid equilibria under high pressure of nine pure *n*-alkylbenzenes *J. Chem. Eng. Data* **53** 233–7

[5] Kruka V R, Cadena E R and Long T E 1995 Cloud-point determination for crude oils *J. Petrol. Technol.* **47** 681–7

[6] Rønningsen H P, Bjørndal B, Hansen A B and Pedersen W B 1991 Wax precipitation from North Sea crude oils: 1. Crystallization and dissolution temperatures, and Newtonian and non-Newtonian flow properties *Energy Fuels* **5** 895–908

[7] Lu Z, Daridon J L, Lagourette B and Ye S 1999 Phase comparison technique for measuring liquid–liquid phase equilibrium *Rev. Sci. Instrum.* **70** 2065–8

[8] Plantier F, Daridon J L and Lagourette B 2003 Measurement of the acoustic nonlinearity parameter in liquid alkanes under pressure and comparison with the Lee–Kesler correlation *High Temp.–High Press.* **35–36** 109–16

[9] Hammami A and Raines M A 1997 Paraffin deposition from crude oils: comparison of laboratory results to field data *Proc. SPE Annual Technical Conf. and Exhibition* Pi pp 273–87

[10] Kok M V, Letoffe J M, Claudy P, Martin D, Garcin M and Volle J L 1996 Comparison of wax appearance temperatures of crude oils by differential scanning calorimetry, thermomicroscopy and viscometry *Fuel* **75** 787–90

[11] Coutinho J A P and Daridon J L 2005 The limitations of the cloud point measurement techniques and the influence of the oil composition on its detection *Petrol. Sci. Technol.* **23** 1113–28

[12] Oliveira N S, Dorgan J, Coutinho J A P, Ferreira A, Daridon J L and Marrucho I M 2006 Gas solubility of carbon dioxide in poly(lactic acid) at high pressures *J. Polym. Sci.* B **44** 1010–9

[13] Oliveira N S, Dorgan J, Coutinho J A P, Ferreira A, Daridon J L and Marrucho I M 2007 Gas solubility of carbon dioxide in poly(lactic acid) at high pressures: thermal treatment effect *J. Polym. Sci.* B **45** 616–25

[14] Ebersole R, Miller J, Moran J and Ward M 1990 PZ quartz sensors for use in clinical analysis *J. Am. Chem. Soc.* **112** 3239

[15] Janshoff A, Galla H J and Steinem C 2000 Piezoelectric mass-sensing devices as biosensors: an alternative to optical biosensors? *Angewandte Chemie Int. Edn.* **39** 4004–32

[16] Sauerbrey G 1955 Verwendung von Schwingquarzen zur Wägung dünner Schichten und zur Mikrowägung *Z. Phys.* **155** 206

[17] Lu C and Czanderna A W 1984 *Application of Piezoelectric Quartz Crystal Microbalance* (New York: Elsevier)

[18] Sauerbrey G 1959 Verwendung von Schwingquarzen zur wägung dünner Schichten und Microwägung *Z. Phys.* **155** 206–22

[19] Wakatsuki N and Kagawa Y 2007 Identification of the properties of a complex layer deposited on the surface of a quartz crystal microbalance (QCM) by the impedance measurement *Meas. Sci. Technol.* **18** 57–61

[20] Kanazawa K K and Gordon J 1985 Frequency of a quartz microbalance in contact with liquid *Anal. Chem.* **57** 1770–1

[21] Kremer F J B, Ringsdorf H, Schuster A, Seitz M and Weberskirch R 1996 Detection of phase transitions in thin

films with a quartz crystal microbalance *Thin Solid Films* **284–285** 436–8
[22] Okahata Y and Ebato H 1989 Application of a quartz-crystal microbalance for detection of phase transitions in liquid crystals and lipid multibilayers *Anal. Chem.* **61** 2185–8
[23] Motorola 1997 MC12061 Datasheet—Crystal Oscillator
[24] Briard A J, Bouroukba M, Petitjean D and Dirand M 2003 Models for estimation of pure *n*-alkanes' thermodynamic properties as a function of carbon chain length *J. Chem. Eng. Data* **48** 1508–16
[25] Ksiazczak A 1989 Vapour pressures of binary three-phase (solid + liquid + vapour) mixtures: II. Melting temperatures of *n*-eicosane phases *J. Chem. Thermodyn.* **21** 789–92
[26] Timmermans J 1965 *Physicochem. Constants Pure Org. Comp.* **2** 1–61
[27] Broadhurst M G 1962 An analysis of the solid-phase behavior of the normal paraffins *J. Res. Natl Bur. Stand.* A **66** 241–9
[28] Doucet J, Denicolo I and Craievich A 1981 X-ray study of the "rotator" phase of the odd-numbered paraffins: C17H36, C19H40 and C21H44 *J. Chem. Phys.* **75** 1523–9
[29] Doucet J, Denicolo I, Craievich A F and Germain C 1984 X-ray study of the rotator phase of paraffins (IV): C27H56, C28H58, C29H60, C30H62 and C34H70 *J. Chem. Phys.* **80** 1647–51
[30] Fredericks R E 1986 Thermal and thermodynamic characteristics of the hydrocarbon components of industrial paraffin waxes *Polymeric Materials Science and Engineering: Proc. ACS Division of Polymeric Material* vol 54 pp 634–7
[31] Schaerer A A, Busso C J, Smith A E and Skinner L B 1955 Properties of pure normal alkanes in the C17 to C36 range *J. Am. Chem. Soc.* **77** 2017–9
[32] Fall D J, Fall J L and Luks K D 1985 Liquid–liquid–vapor immiscibility limits in carbon dioxide + *n*-paraffin mixtures *J. Chem. Eng. Data* **30** 82–8
[33] Fall D J and Luks K D 1984 Phase equilibria behavior of the systems carbon dioxide + *n*-dotriacontane and carbon dioxide + *n*-docosane *J. Chem. Eng. Data* **29** 413–7